IEEE Access
Multidisciplinary | Rapid Review | Open Access Journal

Received September 30, 2020, accepted October 8, 2020, date of publication October 12, 2020, date of current version October 21, 2020.

Digital Object Identifier 10.1109/ACCESS.2020.3030253

Investigation of Stress Wave Interaction and Fragmentation in Granite During Multihole Blastings

CHENGLONG HE[1,2], JINMING GAO[3], DAYONG CHEN[4], AND JIANGUANG XIAO[1,2]

[1]College of Mechatronics Engineering, North University of China, Taiyuan 030051, China
[2]No. 208 Research Institute of China Ordnance Industries, Beijing 102202, China
[3]China Ordnance Engineering and Safety Technology Research Institute, Beijing 100053, China
[4]State Key Laboratory Coal Resources Safe Mining, China University of Mining and Technology, Xuzhou 221000, China

Corresponding author: Chenglong He (hechenglong@nuc.edu.cn)

This work was supported in part by the Natural Science Foundation of Shanxi Province of China under Grant 201901D211278, in part by the Science and Technology Innovation Project of Shanxi Province Colleges of China under Grant 19004417, and in part by the National Natural Science Foundation of China under Grant 11702256 and Grant 51604261.

ABSTRACT Both stress wave superposition and dynamic response process of rock materials are complicated in rock engineering, especially the fracture behavior is difficult to described quantify in the multihole blast loading. The laboratory experiment and a numerical study were performed with granite material to explore stress wave superposition and crack growth in radial and tangential directions. A high-speed photogrammetric system and strain measurement were adopted to obtain the crack propagation and the strain field. The interaction and fragmentation of the stress waves under blasting were simulated. The circumferential tensile stress increased during multihole loading, and the radial cracks further expanded into macroscopic fracture in rock. The development of radial cracks between adjacent holes played a role in rock fracturing. The superposed stress increased nonlinearly with boreholes increased, and both the borehole number and the loading direction influenced the stress field process. The strain field also increased nonlinearly with multihole blasting, and the micro-cracks gradually accumulated. Because of the combined action of the incident and reflected tension waves, the outgoing cracks extended to the boundary along the polygonal path, and the crack branching became seriously around the specimen boundary.

INDEX TERMS Multihole blasting, crack propagation, stress superposition, JH model, digital image correlation.

I. INTRODUCTION

Blasting and drilled boreholes are widely used for many applications. The crack propagation between adjacent holes during multihole blasting are complicated. For single-hole blast loading, shock waves with high pressure act on the borehole and lead to the formation of a crushed zone around the borehole [1], [2]. The shock wave attenuates to stress wave with the increase of the spreading distance, and the tensile tangential stress that follows the compressive stress wave drive the radial cracks growing [3]. Finally, the subsequent explosion gas flow into cracks and drive microcracks to extend further [4]. Recent studies have revealed that the stress waves are responsible for the initiation of the crushing zone and the surrounding radial fractures, and the gas pressure further extends the fractures [5], [6].

For multihole blast loading, the stress wave superposition and dynamic crack propagation are unclear. The interaction process of stress waves are dramatic around the collision point between two adjacent holes, and the tensile stress superposing become strong along the line connected holes [7], [8]. Li *et al.* investigated the effect of empty holes on propagating cracks during blasting, and found that the empty holes had an arrest function on outgoing cracks [9]. Nakamura *et al*. found that stress waves reinforced each other in the region between two charge holes by using polymethyl methacrylate (PMMA) plate experiments [10]. Nakamura captured the shadowgraphs of stress waves interacting with circular holes and researched the effectiveness of guide holes with notches for blast crack control [11]. Yang *et al.* found

The associate editor coordinating the review of this manuscript and approving it for publication was Agustin Leobardo Herrera-May.

that crack growth process were suppressed or promoted when static stress was perpendicular or parallel to the slit direction [12].

The effect of delay times on blast fragmentation is also a research hotspot. The fragment sizes decreased with the delay time in a series of small-scale tests [13]. There were no distinct differences or high improvements for fragmentation when the delays were in the time range of the interactions [14]. Tang *et al.* investigated the effects of the lateral pressure coefficient, overbreak and underbreak, and fault factors on the instability of surrounding rock [15]. Rossmanith *et al.* explored the dynamic crack propagation and bifurcation phenomena by utilizing the strain energy density fracture criterion in the framework of catastrophe theory [16], [17]. The charging structure was also important for the explosion experiment. The detonation wave cannot propagate in charge stably if the charge diameter is lower than the critical diameter of explosive. In the previous references, Simha *et al.* experimented with Plexiglas sheets (305 × 305×50 mm), and the PETN charges were 0.5 g and 10 g/m [18]. S McHugh used cylinder Plexiglas with a size of Φ300 × 300 mm, and the PETN charge had diameters of 3.2 mm (4 g/m) [19]. Rathore *et al.* tested blasts in limestone blocks (550 × 300× Φ250 mm) using an 8.5 g/m detonating cord [20]. Li *et al.* used a sandstone disk (Φ600 × 15 mm) and a PMMA disk (Φ400 × 10 mm), and the charge had a diameter of 6 mm and a density of 1.8 g/cm^3 (50.87 g/m) [9].

Numerical methods have been widely adopted to research the dynamic response of rock materials under blast loading [1], [21]. Li *et al.* presented a dynamic material model for characterizing the dynamic behavior based on the extended Drucker-Prager strength criterion and the JC model [22]. Zhu *et al.* found that shear stress caused a crushed zone near a borehole, and the major tensile principal stress caused a radial crack [23]. Rouabhi *et al.* applied the rate-dependent plasticity theory to simulate the dynamic fragmentation in blasting [24]. Ma *et al.* found that only a crushed zone was created when the loading rate was very high [25]. Karrech *et al.* introduced a constitutive hydraulic model based on non-equilibrium thermodynamics, and found that damage evolution lead to an inhomogeneous redistribution of material properties and also provided new insights into energy evolution during longwall mining [26], [27].

This research was focused on the stress wave superposition and crack growth in radial and circumferential directions during multihole blasting. In experimental studies, the granite specimens composed of square plates containing 1-4 holes and #5 cotton detonating cord were selected. A High speed (HS) camera, Digital Image Correlation (DIC), and strain measurement were adopted to obtain the crack propagation and strain field in the radial and circumferential directions. Based on the Johnson-Holmquist (JH) constitutive model, the stress wave interactions and the radial crack propagation for multihole blasting were simulated in AUTODYN hydrocode.

II. METHODS AND MATERIALS

A. EXPERIMENTAL SET UP

The granite samples were selected from the same parent rock from Shandong, China. Based on the International Society for Rock Mechanics (ISRM) standards, the parallelism and the perpendicularity were lower than 0.2 mm. The quasi-static properties of granite were tested in the Laboratory of Explosion at the Beijing Institute of Technology. The property parameters of the granite were as follows. The tensile strength was 7.64 MPa, the compressive strength was 86.62 MPa, the density was 2.66 g/cm^3, Poisson's ratio was 0.2, and Young's modulus was 36.8 GPa. The sample size was 360 × 360×100 mm (height, width, and thickness), and the non-penetrative borehole with a 90 mm depth was designed to prevent the explosion gas overflowing from the borehole. The multihole blasting included single-, two-, three-, and four-hole loading, corresponding to specimens 1-4 (Fig. 1).

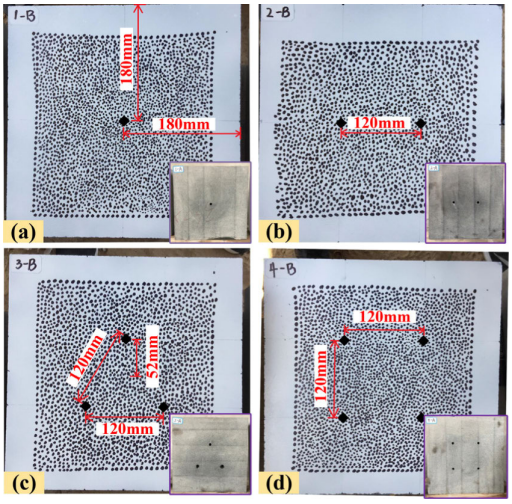

FIGURE 1. The location of the boreholes in specimens 1-4: (a) specimen 1; (b) specimen 2; (c) specimen 3; (d) specimen 4.

The strain sensors were pasted on the back faces (A) of the specimens, and the front faces (B) were used for the HS camera test. The locations of the strain gauges are shown in Fig. 2. Two orthogonal gauges were set up in each test point. The DC power (4 V) and the Wheatstone bridge for signal amplification were adopted in the strain test system. The strains were extracted from the measured signals using bridge amplification and the calibrated gauge factor. The total amplification factor was 400, and the strain increase was 0.001 when the output voltage increased by 0.4 V. The strain gauge signals were recorded with a High dynamic strain indicator with a 10 M sampling rate (10 signals were recorded every microsecond). The synchronization trigger units were built to trigger the strain test system and the high-speed camera.

Based on the above research results, #5 cotton detonating cord with 6 mm diameter (10.5 g/m) was used in the experiments. The PETN charges of the 1.0 g/cm^3 detonating

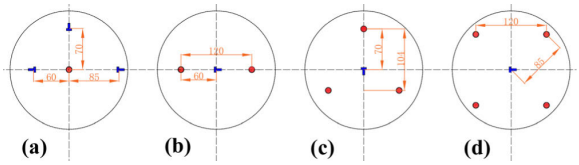

FIGURE 2. Strain gauge positions in the four specimens: (a) three test points in specimen 1; (b) one test point in specimen 2; (c) one test point in specimen 3; (d) one test point in specimen 4.

cord was 3.6 mm diameter, and the detonation velocity was 6000 m/s. The cylindrical charge was covered by red cotton, and both the plastic tube (Φ9.6 mm) and the adhesive tape were used to fix the PETN charge (Fig. 3). The air-uncouple charge construction was selected to reduce the shock wave, and the spacing distance was 1.8 mm. The electric discharge method was adopted to inspire the synchronization trigger system.

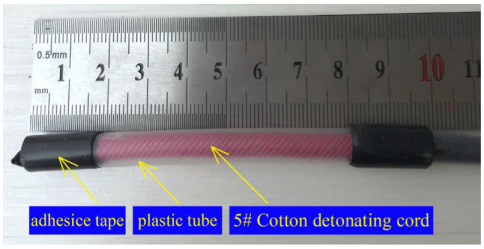

FIGURE 3. Structure of the #5 cotton detonating cord.

Many techniques have been developed for detecting the crack growth in brittle materials under dynamic loading [28]. Digital image correlation as a non-contact measurement has been widely used to investigate crack propagation in blasting experiments [29], [30]. Zhu *et al.* used DIC and acoustic emission (AE) techniques to record and analyze the deformation and crack process of rock materials [31], [32]. In this study, the 2D-DIC method was selected, the real-time images of the loaded specimen were captured by a high-speed camera with 62,500 frames per second (fps), and the interval time between two images was 16 μs. As shown in Fig. 4, size of the area of interest (AOI) was 206 × 206 mm with 320 × 320 pixels. The speckle pattern was randomly distributed in a proper density with good contrast. The Photron^{TM}High Speed Camera FASTCAM SA5 was set up with Nikon lenses, and two high-strength glass were set up to protect light-emitting diode (LED) lights. The Von Mises strain fields were calculated using Vic-2D software (the subset was 9, and the step was 2).

B. NUMERCAL MODEL

Numerical analyses have proven to be a useful tool in helping investigations when costs and security issues require limiting experimental campaigns [33], [34]. The AUTODYN finite element model has been widely applied in solving rock fracturing under dynamic loading. The JH model considers most of the material parameters of brittle materials subjected to large strains, high strain rate, and high pressures. A polynomial state equation which selected to describe the nonlinear

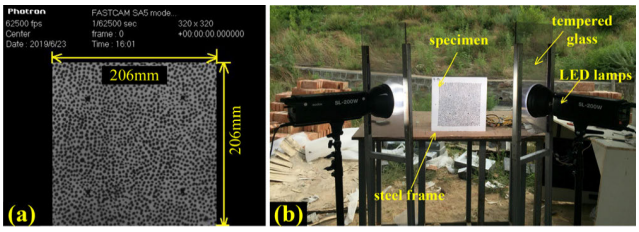

FIGURE 4. Experiment photographs: (a) AOI area; (b) Schematic diagram of the experiment.

compressibility when shock waves transmit into rock materials, the relation between pressure (P) and relative volume (μ) is expressed as:

$$P = k_1\mu + k_2\mu^2 + k_3\mu^3 + \Delta P \quad \text{for compression condition} \tag{1}$$

$$P = k_1\mu + k_2\mu^2 \quad \text{for tension condition} \tag{2}$$

where, $\mu = \rho/\rho_0 - 1$, ρ represents current density, ρ_0 is reference density, and ΔP is an additional pressure increment determined from energy considerations to include the dilatation effect after compression failure. K_1 is the bulk modulus, K_2 and K_3 are constants.

Based on the polynomial state equation, the Hugoniot Elastic Limit (*HEL*) and the pressure on the HEL point (P_{HEL}) represent as:

$$\begin{cases} HEL = K_1\mu_{HEL} + K_2\mu_{HEL}^2 + K_3\mu_{HEL}^3 \\ \quad + \dfrac{4}{3}G\left(\dfrac{\mu_{HEL}}{1+\mu_{HEL}}\right) \\ P_{HEL} = K_1\mu_{HEL} + K_2\mu_{HEL}^2 + K_3\mu_{HEL}^3 \end{cases} \tag{3}$$

$K_1 = \frac{E}{3(1-2\upsilon)} = \frac{36.8}{3(1-2\times0.2)} = 20.45$ GPa$G = \frac{E}{2(1+\upsilon)} = \frac{36.8}{2(1+0.2)} = 15.33$GPa, K_2, K_3, μ_{HEL} are − 4500 GPa, 3e5GPa, 0.028 (three values are obtained based on related references [35], [36]). Hugoniot Elastic Limit (*HEL*), *Hydro Tensile Limit*=T$*$ × P_{HEL} =50.82 MPa ($T*$ =0.014), the *HEL* were sued in the Johnson-Holmquist failure model. The results of the static experimental results were used for the calibration of the parameters of the JH model based on reference [37]. The parameters are shown in Table 1.

The rock model and the PETN charge structure were built based on the experiment, the PETN cylinder charge were built with 3.6 mm diameter, the borehole was 10 mm diameter, and red cotton, plastic tube were not added in simulation. The JWL equation was used for the hydrodynamics of the explosive detonation. The number of rock elements was approximately 360,000 (0.6 mm length), and the Euler grids were approximately 57,600. The total analyzed time was 120 μs, and the key points were selected based on the strain gauge positions (60 mm, 70 mm, and 85 mm from the borehole).

III. EXPERIMENTAL RESULTS

A. DYNAMIC STRAIN IN THE RADIAL AND CIRCUMFERENTIAL DIRECTIONS

Four experiments were performed in the Laboratory of Explosion at the Beijing Institute of Technology. Using the strain

TABLE 1. Parameters of the JH constitutive model.

Parameters		Unit	Value
Equation of state			
Reference density	ρ_0	(g/cm^3)	2.66
Bulk modulus	K_1	(GPa)	20.45
Polynomial EOS constant	K_2	(GPa)	-4500
Polynomial EOS constant	K_3	(GPa)	300,000
Johnson-Holmquist strength model			
Shear modulus	G	(GPa)	15.33
Hugoniot Elastic Limit	HEL	(GPa)	4.19
Intact Strength Constant	A		0.97
Intact Strength Exponent	N		0.64
Strain Rate Constant	C		0.005
Fractured Strength Constant	B		0.32
Fractured Strength Exponent	M		0.64
Max. Fractured Strength Ratio	σ^*_{FMax}		0.25
Johnson-Holmquist failure model			
Hydro Tensile Limit	$T^*\times P_{HEL}$	(GPa)	-51
Damage constant	D_1		0.005
Damage constant	D_2		0.70
Bulking constant	β		0.50
Type of tensile failure			Hydro

gage to acquire deformation directly was an effective method to describe failure process, the elastic deformation were produced if the strain returned to zero after peak value, and the irreversible inelastic strains occurred if the strain did not returned to zero after peak value. Fig. 5 displayed the deformational process at 60 mm, 70 mm, and 85 mm in specimen 1 with single hole blasting. The strainXX (ε_{xx}) and strainYY (ε_{yy}) described the radial and circumferential deformation, and the stress wave propagated along the coordinate axis. The rock dynamic strength increased with the loading rate, and there was no theoretical model to accurately estimate the dynamic strength during blast loading. According to previous studies, the dynamic compressive and tensile failure strains were estimated to be 0.007 and 0.0015, respectively.

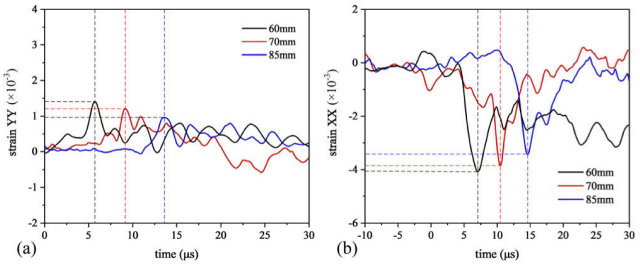

FIGURE 5. Strain-time curves at 60 mm, 70 mm, and 85 mm in specimen 1: (a) ε_{yy}; (b) ε_{xx}.

ε_{yy} was over zero, and the tensile deformation played a role in the circumferential destruction (Fig. 5a). The stress wave propagated outward at about 3000 m/s, and the average duration time of stress wave was 4 μs. The strain peaks for 60 mm, 70 mm, and 85 mm reached 1.44×10^{-3}, 1.20×10^{-3}, and 0.96×10^{-3} at 5.6 μs, 9.3 μs, and 13.8 μs after the PETN detonated, respectively. The circumferential tensile stress caused radial fissures at 60 mm when ε_{yy} exceeded the rock failure tensile strain. The elastic deformation gradually replaced the plastic deformation with the increase of the spreading distance.

ε_{xx} was lower than zero, and the compressive deformation was produced in the radial direction (Fig. 5b). The extreme values at the 60 mm, 70 mm, and 85 mm points were -4.05×10^{-3}, -3.80×10^{-3}, and -3.40×10^{-3}, corresponding to 7.0 μs, 10.5 μs, and 14.6 μs, respectively. The extreme strain at 60 mm was -0.00405, and it did not exceed the dynamic compressive strain (-0.007). The results showed that the circumferential tensile fractures were seriously than the radial compression failure.

The superimposed deformations along the X,Y axis are shown in Fig. 6 and Fig. 7. The dynamic responses of specimens 1-4 were compared at 60 mm, 70 mm, and 85 mm. ε_{xx} and ε_{yy} described radial and circumferential deformation only in specimens 1 and 2, because the propagation direction of the blast loadings was either orthogonal or parallel with the strain gauges.

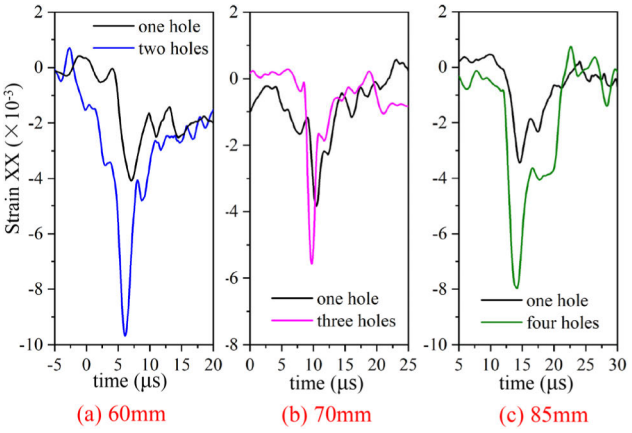

FIGURE 6. Deformation along the X-axis: (a) specimens 1 and 2; (b) specimens 1 and 3; (c) specimens 1 and 4.

For the two symmetrical blasting in specimen 2, ε_{xx} was -0.0097, which was 2.5 times greater than the value of specimen 1 (-0.004), as shown in Fig. 6a. The reinforced ratio was greater than 2 in specimen 2, which indicated that the reinforce effect did not increase linearly with the blasting number. The reinforcement became weak for the unsymmetrical stress waves in specimens 3 and 4, and the reinforced ratio was lower than 2 for the three-hole and four-hole blasting (Fig. 6b, c).

As shown in Fig. 7, the reinforcement of the tensile deformation along the circumferential direction was not significant

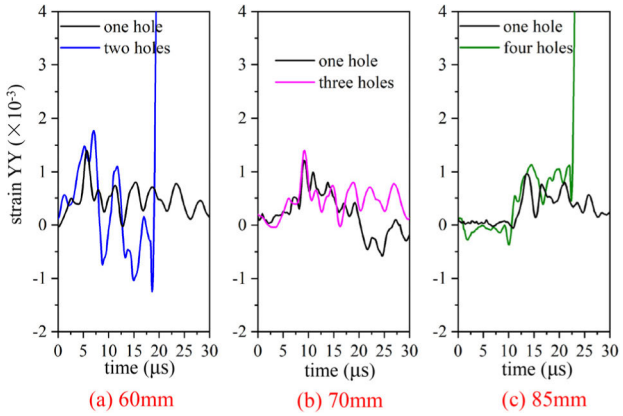

FIGURE 7. Deformation along the Y-axis: (a) specimens 1 and 2; (b) specimens 1 and 3; (c) specimens 1 and 4.

in specimen 2. The strain peak of specimen 2 reached 0.0017, which was 1.2 times the peak of specimen 1. The results were attributed to the plastic deformation increasing nonlinearly for multiple loading. Additionally, radial cracks started to accumulate when the strain exceeded the limit tensile strain. The strain gauge was failed at 19 μs (Fig. 7a), and the radial cracks were extant between two holes for the circumferential tensile stress. The dynamic responses of specimens 1 and 3 were similar, as shown in Fig. 7b. For specimen 4, ε_{yy} reached 0.0011 at 14 μs and exceeded the acceptable range at 24 μs (Fig. 7c).

B. DYNAMIC RESPONSE WITH DIC

Fig. 8 displayed the evolution of the Von Mises strain field in specimen 4 for four-multihole blasting. The total analysis time was 80 μs. The area of the strain contours was 206 × 206 mm, and it consisted of an original image and a calculated picture with 20% opacity. It should be noted that the time did not start at the triggering time, but rather started at the deformation of the specimen.

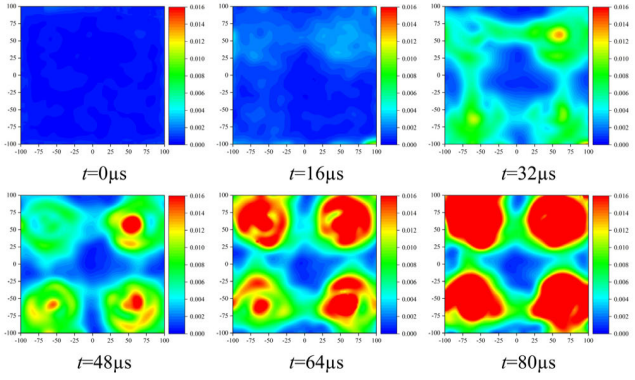

FIGURE 8. Strain field from the DIC results in specimen 4 (t=16 μs, total time was 80 μs).

The shock waves originated from the boreholes after detonation, and the strain around the right-up hole was over 0.01 at 32 μs. Smaller cracks were densely populated near the borehole and formed the crushing zone. Four orthogonal strain bands connected holes, and the strain peak was less than 0.01 (Fig. 8). As the time increased to 48 μs, the deformation close to borehole was over 0.016, which was higher than the rock strength. Moreover, the calculated strain was not accurate when the strain exceeded 0.016 because the rock particles from the hole bottom reduced the visibility of the photograph. The fracturing became observable around the holes at 64 μs, but the strain band between holes was not reinforced. At 80 μs, the tiny particles flew from the bottom of the borehole, resulting in the crack growth not being observed clearly.

The evolution of the strain field were influenced by two factors during blasting. The first factor was the spalling, which was caused by the reflected waves along the free surface and the deformation perpendicular to the surface exaggerating the strain field in the front surface. Another factor was that the flying particles from the hole bottom were captured by a camera, and the accuracy of the computed strain was reduced by the DIC analysis.

Fig. 9 clearly exhibited the failure process for the high-speed photographs in specimen 4 with the four-borehole blasting. The deformations were produced by the stress waves before 64 μs, and the radial cracks were not clearly between holes. The results showed that the spread of the crack was slower than the stress wave propagation. The explosion gases with high pressure and temperature flew out from the borehole after 80 μs and made the fracturing more seriously with the time increase. Because the explosive gases reduced the sharpness of the photos, the strain field could not be analyzed at the end.

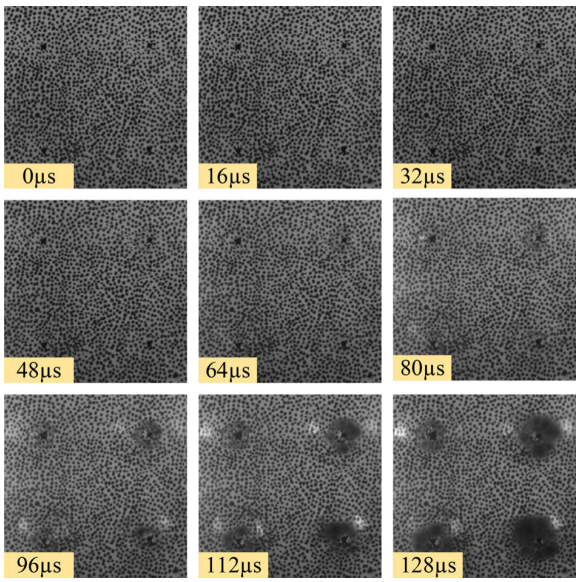

FIGURE 9. Specimen 4 failure process for high-speed photographs.

C. FRAGMENTATION IN FOUR SPECIMENTS

Fig. 10 displayed the crack patterns in the photographed plane in specimens 1-3. The partial cracks were magnified

into view. The fragment collection of specimen 4 failed after blasting because the fragments were smaller, and they spread everywhere with high speed. The cracks were clearly observed in the front surface. The fracturing damage was significant around the borehole in the three specimens. The results were caused by the tensile failure along the free surface.

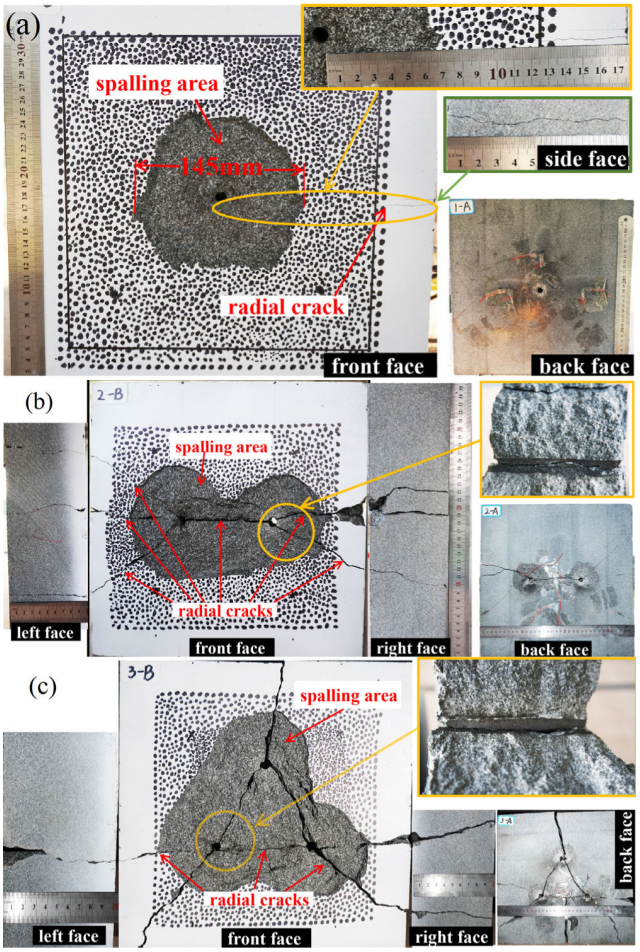

FIGURE 10. Fragmentation in specimens after blasting: (a) specimen 1; (b) specimen 2; (c) specimen 3.

The fragmentation of specimen 1 were exhibited in the front, side, and the back face (Fig. 10a). The fracturing area that was closed to the center hole had a diameter of 145 mm and a depth of 4 mm. The borehole wall and the crushed area were slightly damaged because the air-uncouple charge reduced the shock wave along the borehole. A radial crack started from the central hole and extended to the specimen's right boundary at the end. The crack path in the front and back faces was similar, and the shock wave from the detonating cord acted evenly on the borehole. For the reflected tension wave from the free boundary, the radial crack became wide when it was close to the boundary.

Fig. 10b presents the damage of specimen 2. The spalling area increased along the horizontal direction and became the depth (6 mm) between holes. The horizontal predominant radial cracks extended to the boundary. Moreover, the right crack branched into two cracks at 55 mm from the right boundary. Only one horizontal crack connected two holes, and three outgoing cracks started from the borehole and extended to the boundary. The results showed that the reflected wave had a great effect on the growth of the radial crack. The vertical penetrating cracks were not found because the burden distances between the borehole and the up-down boundary were greater than those in the horizontal direction.

The fracturing became more serious with the borehole increase in specimen 3 (Fig. 10c). Three main cracks connected the holes, and the macrofissures were not produced in the center-triangle region. The phenomenon suggested that more explosive energy was used for the radial cracks that developed between holes. One crack originated from the upper hole and extended to the specimen's upper boundary, and two cracks started from the two bottom holes to the left-right boundary. The crack patterns of specimen 3 were similar to those of specimen 2, and the number and pathways of the outgoing radial cracks were influenced by the distance between the hole and the boundary.

IV. SIMULATION RESULTS

A. STRESS FIELD EVOLUTION FOR MULTIHOLE LOADINGS

Fig. 11 shown the Von Mises stress field in the four specimens. The reflected waves were generated close to the boundary at 40 μs, and cracks stop developing at 120 μs. The central symmetry stress wave originated from the central borehole in specimen 1 at 20 μs, and the stress around the hole wall arrived at 140 MPa and exceeded the rock dynamic strength (Fig. 11a). Radial cracks were randomly distributed near the borehole during the stress wave. After 60 μs, the reflected wave from the free boundary drove the radial cracks to grow further in the vertical and horizontal directions.

The stress superposition were obviously in the central zone between the two holes in specimen 2 (Fig. 11b). The crack tip stress field became stronger for blasting for two holes. The radial crack formed the left hole and extended to the right hole, and then it bifurcated into two cracks in the central zone. The branch cracks problems of boundary region became complicated because the superposing process of stress waves were unclear. The left and right cracks met each other and merged at 80 μs. The horizontal crack ran though specimen 2 under the reflected wave, and this phenomenon agreed with the experimental results.

The superposed stress closed to the central point did not become strong at 20 μs in specimen 3 (Fig. 11c). The stress dropped to zero, and no cracks appeared in the central zone. Instead, the stress concentration were obviously between holes, and driven radial cracks developing. In specimen 3, two cracks extended to the upper, left, and right boundaries. Under the combined action of the initial and reflected tension waves, the crack branching was obviously near the free boundary, especially in the corner position. The stress concentration between two holes were also observed clearly in specimen 4

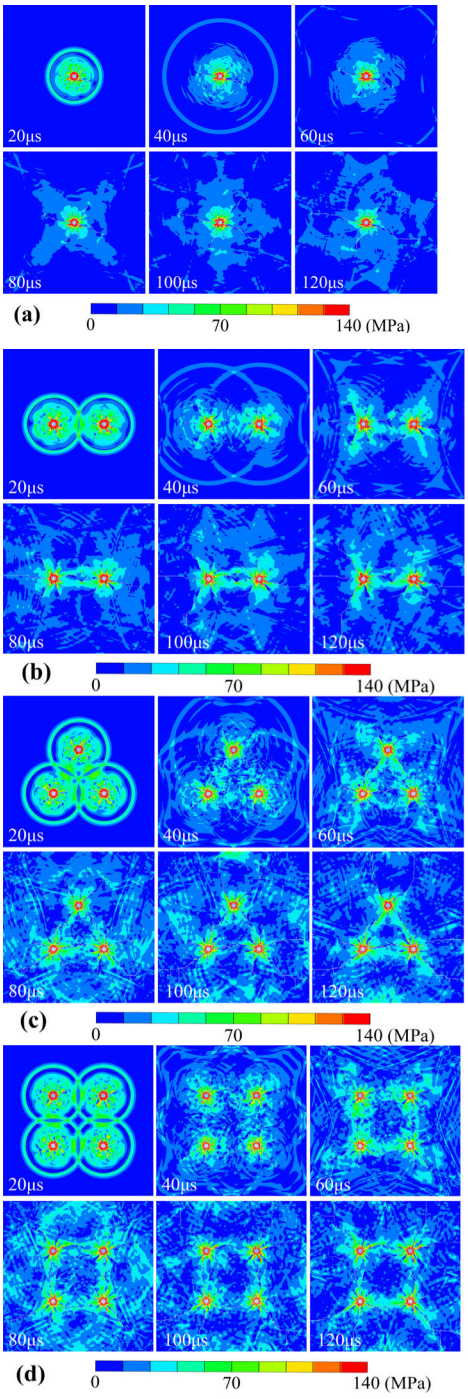

FIGURE 11. Von Mises stress field for multihole blasting: (a) specimen 1; (b) specimen 2; (c) specimen 3; (d) specimen 4.

(Fig. 11d), but the cracks were still not found in the center area. The phenomenon further illustrated the fact that the circumferential tensile fracture played an important role in the rock breaking process.

To quantitatively analyze the superposing process of the Von Mises stress in the four specimens, the stress-time curves at 10-30 μs were selected in Fig. 12. Fig. 12a compared the stress field at 60 mm for single-hole and double-hole blasting. The stress wave arrived 60 mm at 13 μs and sharply increased

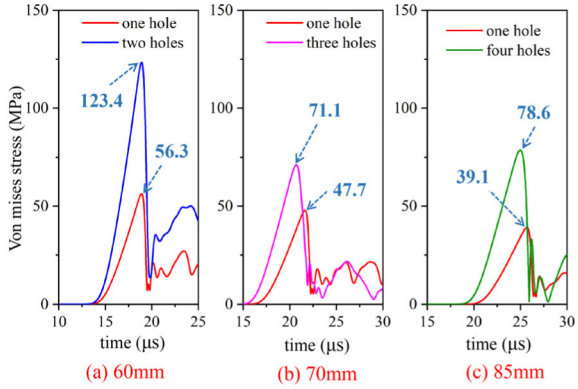

FIGURE 12. Von Mises stress-time curves at 10-30 μs: (a) specimens 1 and 2; (b) specimens 1 and 3; (c) specimens 1 and 4.

to 123.4 MPa at 16 μs for double-hole loading. The peak value of specimen 2 was higher than it in specimen 1, and the wavelength was 5 μs, which was not affected by the amount of blasting. The peak stresses of the central point arrived at 71.1 MPa and 78.6 MPa for two and three holes (Fig. 12b,c), and both were lower than the peak value in specimen 2. The dynamic stresses of specimens 3 and 4 did not increase proportionally, and the superposing stresses were not completely controlled by the multihole blasting numbers. Both the blasting number and the loading direction influenced the development of the stress field.

B. DYNAMIC RESPONSE ALONG X, Y DIRECTION

The Von Mises stress did not increase with the borehole numbers, as described in Section 4.1. This section describes the stress components along the X,Y axis. Fig. 13 shows ε_{yy} and ε_{xx} at 35 μs for the initial stress waves, and the reflected wave was not produced before 35 μs.

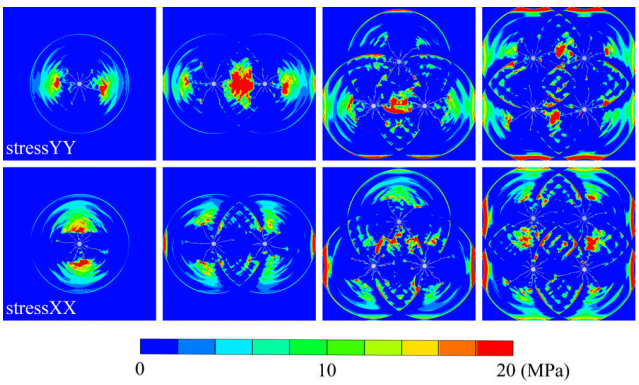

FIGURE 13. Stress fields of stressYY and stressXX at 35 μs.

ε_{yy} exceeded 20 MPa, and the radial cracks developed along the horizontal direction for the circumferential tensile stress. The strain concentration were seriously at the horizontal crack tip, especially in the central damage zone between the two holes in specimen 2. The upper and lower cracks in specimens 3 and 4 obviously grew along the horizontal direction. A similar phenomenon happened in ε_{xx} field; the

radial cracks developed in a long vertical direction due to the circumferential tensile stress. The superimposed stress waves were smaller between the two holes in specimen 2, which caused the vertical cracks to stop in the crushing zone.

The reflected waves were produced along the free boundary after 60 μs, and the propagation of outgoing cracks from the borehole was controlled, as shown in Fig. 14. ε_{xx} around horizontal crack tip became strongly, and the stress concentration area were irregular under initial and reflected waves. A similar phenomenon also occurred in the strain field, and the outgoing cracks extended along the vertical direction. The problematic bifurcated cracks became very close to the free boundary, especially in the corner position.

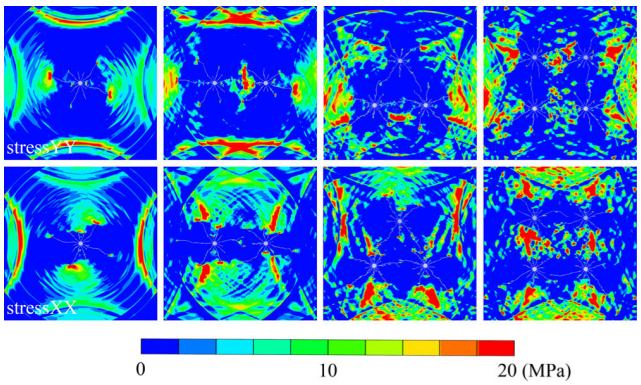

FIGURE 14. Stress field of stressYY and stressXX at 60 μs.

It should be noted that stressXX and stressYY described radial and circumferential deformation at 60 mm only in specimens 1 and 2, as shown in Fig. 15 and Fig. 16.

ε_{xx} were compressive at 15-19 μs, and they reached -110.8 MPa in specimen 2, which was double the value of specimen 1 (Fig. 15a). The tensile wave followed the compression waves during 19-21 μs, and this phenomenon was not obvious in the experimental strain signals (see Fig. 6). Because the loading directions were not orthogonal to the test points, the reinforcement effect of ε_{xx} became weakly in specimens 3 and 4 (Fig. 15b, c). It was also noteworthy that the four stress waves overlaid each other and caused ε_{xx} to rise to 64.8 MPa in specimen 4, but ε_{xx} could not be used to judge whether the tensile fracture occurred.

The compressive ε_{yy} were not significant in the stressYY-time curves in specimens 1 and 2. This phenomenon were similar to the experimental results, as shown in Fig. 16a. The reinforcement of the tensile ε_{yy} became stronger in specimen 2, and ε_{yy} did not drop to zero, indicating that the plastic deformation was produced by tensile loading. For multiple loadings in specimens 3 and 4, both ε_{yy} nadir and the peak increased with the loading times.

V. DISCUSSION

A. DYNAMIC STRAIN IN THE EXPERIMENTAL AND NUMERICAL RESULTS

Fig. 17 represented strainXX and strainYY at three test points from the numerical results. In the radial direction,

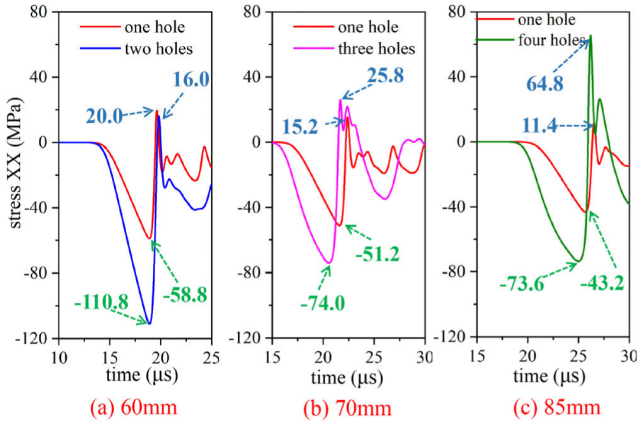

FIGURE 15. Superimposed stressXX-time curves: (a) specimens 1 and 2; (b) specimens 1 and 3; (c) specimens 1 and 4.

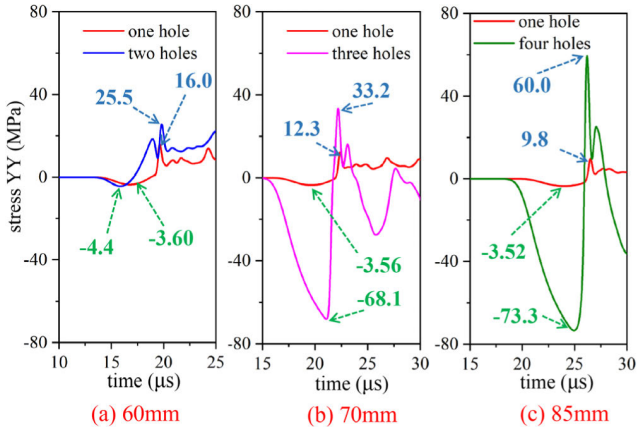

FIGURE 16. Superimposed stressYY-time curves: (a) specimens 1 and 2; (b) specimens 1 and 3; (c) specimens 1 and 4.

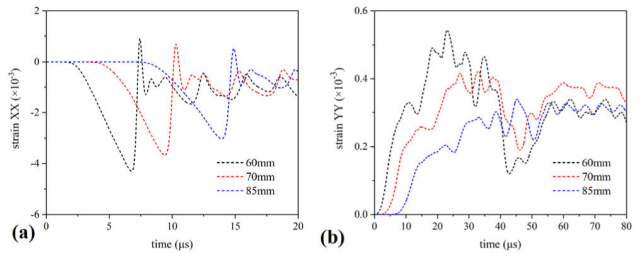

FIGURE 17. StrainXX and strainYY at three points from the numerical results. (a) StrainXX; (b) strainYY.

the compressive deformation were produced and then became the tensile deformation, and strain fluctuated around zero value in the end (Fig. 17a). The elastic deformation played a role in dynamic response, strainXX was reduced gradually and the deformation increased with the distance increased. Different from strainXX curves, strainYY were greater than zero and the tensile deformation lasted about 40μs which was eight times than strainXX in Fig. 17b. The strain peak decreased with the spreading distance increased, and strainYY fluctuated around 0.0003.

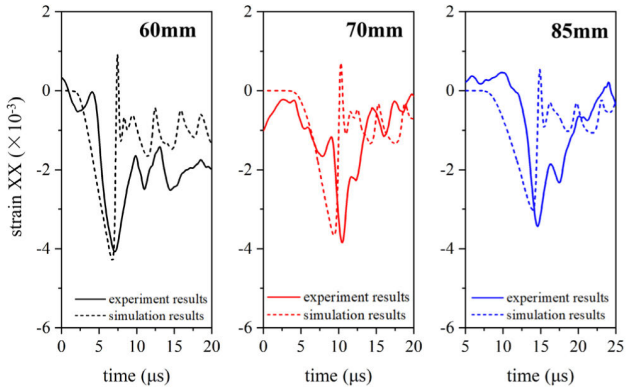

FIGURE 18. StrainXX-time curves at 60mm, 70mm, 85mm from experimental and numerical results.

The radial strainXX were negative firstly and then positive in the numerical results, but this tendency were not found in experimental results (Fig. 18). This happens because the interaction of stress waves along free surface were complicated, and further caused strain signals fluctuating in experimental results. Moreover, the time of deformation in experimental results were obviously longer than that from numerical results. Both the experimental numerical results indicated that the compressive strain played important role in radial damage.

Fig. 19 described the strainYY-time curves between experimental and numerical results. Compared with strain from experimental results, strainYY were smaller and last longer in numerical results. Because the accumulation of plastic strain gradually increased when the equivalent stresses exceeded the elastic limit strength of the rock, and the damage were calculated by accumulated equivalent plastic strain. The brittle rupture process in experimental results were fast compared the numerical results.

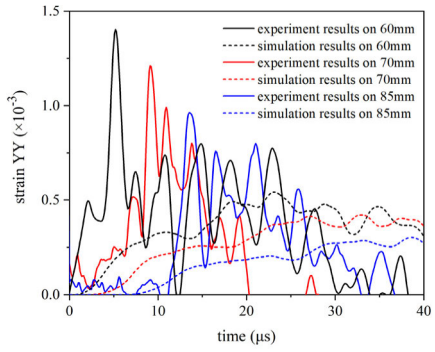

FIGURE 19. StrainYY-time curves at 60mm, 70mm, 85mm from experimental and numerical results.

B. CRACK PATTERNS

The fractures were easily observed in the specimen's back face (Fig. 20), and the fragments were produced along the free surface in the three specimens. There were one and two main cracks between the holes in specimen 2 and in specimen 3, respectively. The outgoing cracks extended to the free boundary with the help of the reflected tension stress wave. Under the combined action of the initial and reflected stress waves, the left crack in specimen 2 branched into two cracks near the left boundary.

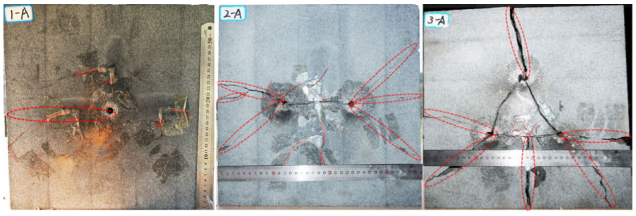

FIGURE 20. Fragmentation in the back surface of specimen 3.

The simulated results were shown in Fig. 21. The crack patterns agreed with the experiment results. Compared to the fracturing around the borehole in the simulation results, the number of radial cracks was greater than that in the experiment results because the two-dimensional model did not consider the escaped explosive energy from the bottom holes in the simulation. The dynamic branch were seriously around the four corners of specimens 3 and 4, but the crack branching process were not a common phenomenon in the experiment results.

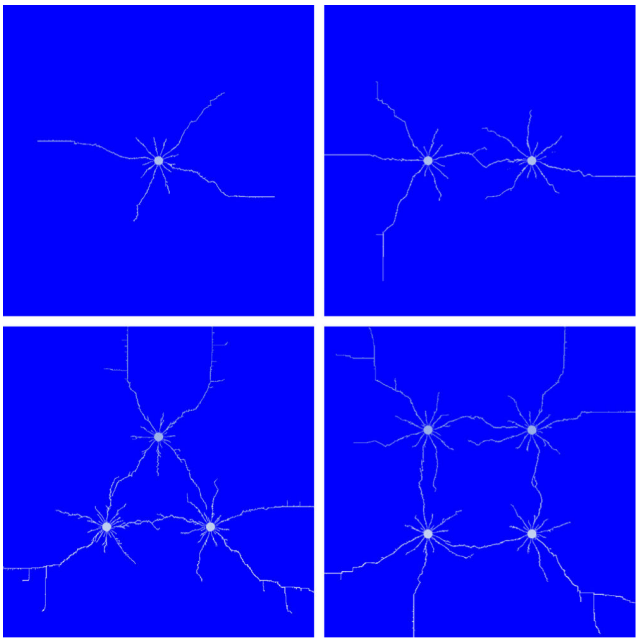

FIGURE 21. Crack patterns in the simulated results.

VI. CONCLUSION

The dynamic response process of rock materials under interacted stress waves is a complex dynamical mechanics problem, especially the fracture behavior is difficult to described quantify. To investigate the stress wave superposition and crack growth in the radial and tangential directions during

multihole blasting, experimental and numerical studies were performed. Four laboratory experiments were performed using granite specimens of square plate containing 1–4 holes, and #5 cotton detonating cord and an air-uncouple charge were selected to reduce the shock wave. An HS camera, the DIC method, and strain measurement were adopted to obtain the crack propagation and the strain field. Based on the JH model, the interaction of the stress waves and the radial crack propagation for multihole blasting were simulated in AUTODYN hydrocode.

During air-uncouple blasting, both the borehole wall and the radial fracturing near the borehole were damaged slightly. The fracturing and flying particles reduced the accuracy of the computed strain field based on DIC analysis. The superposition of the circumferential tensile stress drove the radial cracks connecting adjacent boreholes, which played a role in the fragmentation in the central damage zone. The reinforcement effect of the stress waves did not increase linearly with the blasting numbers. The strain field also increased nonlinearly with the loading times because plastic deformation appeared when the strain exceeded elastic limit. The extension of the outgoing cracks to the boundary was influenced by the reflected tension wave. Both the burden distance and the boundary shape controlled the pathways of the outgoing cracks. The crack branching became very close to the free boundary, especially in the corner position.

In the simulated results, the strengthening effects and the crack patterns were in agreement with the experiment results. The growth of the cracks between adjacent boreholes due to circumferential tensile stress played an important role in the rock breaking. The brittle rupture process in experimental results were fast compared the numerical results, because the damage were calculated by accumulated plastic strain. The number of radial cracks was more than that in the experiment results because the escaped explosive energy was not considered in the two-dimensional model. The branch crack problems were serious around the specimen's four corners in the simulated results.

REFERENCES

[1] L. Y. Chi, Z.-X. Zhang, A. Aalberg, J. Yang, and C. C. Li, "Measurement of shock pressure and shock-wave attenuation near a blast hole in rock," *Int. J. Impact Eng.*, vol. 125, pp. 27–38, Mar. 2019.

[2] J. F. Labuz, S. P. Shah, and C. H. Dowding, "Experimental analysis of crack propagation in granite," *Int. J. Rock Mech. Mining Sci. Geomech. Abstr.*, vol. 22, no. 2, pp. 85–98, 1985, doi: 10.1016/0148-9062(85)92330-7.

[3] W. I. Duvall and T. C. Atchison, *Rock Breakage by Explosives*, vol. 5356. Washington, DC, USA: US Bureau of Mines, 1983.

[4] A. R. Cameron, "Development of techniques for evaluating the performance of bulk commercial explosives," *Published Online*, to be published.

[5] C. H. Dowding and C. T. Aimone, "Multiple blast-hole stresses and measured fragmentation," *Rock Mech. Rock Eng.*, vol. 18, no. 1, pp. 17–36, 1985.

[6] X. Ding, W. Zhou, X. Lu, M. Li, E. Manda, X. Shi, B. Luan, and C. Qi, "Distribution characteristics of fragments size and optimization of blasting parameters under blasting impact load in open-pit mine," *IEEE Access*, vol. 7, pp. 137501–137516, 2019.

[7] L. Yang, C. Ding, R. Yang, and Q. Wang, "Experimental and theoretical analysis of stress superposition in double-hole blasts," *J. Test. Eval.*, vol. 48, no. 5, Sep. 2020, Art. no. 20180093.

[8] C. Yi, D. Johansson, U. Nyberg, and A. Beyglou, "Stress wave interaction between two adjacent blast holes," *Rock Mech. Rock Eng.*, vol. 49, no. 5, pp. 1803–1812, May 2016, doi: 10.1007/s00603-015-0876-x.

[9] M. Li, Z. Zhu, R. Liu, B. Liu, L. Zhou, and Y. Dong, "Study of the effect of empty holes on propagating cracks under blasting loads," *Int. J. Rock Mech. Mining Sci.*, vol. 103, pp. 186–194, Mar. 2018, doi: 10.1016/j.ijrmms.2018.01.043.

[10] Y. Nakamura, S. H. Cho, M. Yoneoka, M. Yamamoto, and K. Kaneko, "Model experiments on crack propagation between two charge holes in blasting," *Sci. Technol. Energetic Mater.*, vol. 65, pp. 34–39, Apr. 2004.

[11] Y. Nakamura, "Visualization of stress waves in blasting processes by a laser-shadowgraph method and its applications to dynamic fracture control," in *Proc. 8th Int. Congr. Exp. Mech.*, vol. 272, 1996.

[12] R. Yang, C. Ding, L. Yang, Z. Lei, and C. Zheng, "Study of decoupled charge blasting based on high-speed digital image correlation method," *Tunnelling Underground Space Technol.*, vol. 83, pp. 51–59, Jan. 2019, doi: 10.1016/j.tust.2018.09.031.

[13] P. D. Katsabanis, A. Tawadrous, C. Braun, and C. Kennedy, "Timing effects on the fragmentation of small scale blocks of granodiorite," *Fragblast*, vol. 10, nos. 1–2, pp. 83–93, Mar. 2006.

[14] D. Johansson and F. Ouchterlony, "Shock wave interactions in rock blasting: The use of short delays to improve fragmentation in model-scale," *Rock Mech. Rock Eng.*, vol. 46, no. 1, pp. 1–18, Jan. 2013.

[15] Z. Tang, W. Yao, J. Zhang, Q. Xu, and K. Xia, "Experimental evaluation of PMMA simulated tunnel stability under dynamic disturbance using digital image correlation," *Tunnelling Underground Space Technol.*, vol. 92, Oct. 2019, Art. no. 103039, doi: 10.1016/j.tust.2019.103039.

[16] K. Uenishi and H. P. Rossmanith, "Stability of dynamically propagating cracks in brittle materials," *Acta Mechanica*, vol. 156, nos. 3–4, pp. 179–192, Sep. 2002.

[17] H. P. Rossmanith and W. L. Fourney, "Fracture initiation and stress wave diffraction at cracked interfaces in layered media I. Brittle/brittle transition," *Rock Mech. Felsmechanik Mécanique des Roches*, vol. 14, no. 4, pp. 209–233, Feb. 1982.

[18] K. R. Y. Simha, W. L. Fourney, and R. D. Dick, "Studies on explosively driven cracks under confining *in-situ* stresses," in *Proc. Symp. Rock Mech.*, 1984, pp. 933–941.

[19] S. McHugh, "Crack extension caused by internal gas pressure compared with extension caused by tensile stress," *Int. J. Fract.*, vol. 21, no. 3, pp. 163–176, Mar. 1983, doi: 10.1007/BF00963386.

[20] S. S. Rathore and S. Bhandari, "Controlled fracture growth by blasting while protecting damages to remaining rock," *Rock Mech. Rock Eng.*, vol. 40, no. 3, pp. 317–326, Jun. 2007.

[21] J. Song and K. Kim, "Micromechanical modeling of the dynamic fracture process during rock blasting," *Int. J. Rock Mech. Mining Sci. Geomech. Abstr.*, vol. 33, no. 4, pp. 387–391, 1996, doi: 10.1016/0148-9062(95)00072-0.

[22] H. Y. Li and G. Y. Shi, "A dynamic material model for rock materials under conditions of high confining pressures and high strain rates," *Int. J. Impact Eng.*, vol. 89, pp. 38–48, Mar. 2016.

[23] Z. Zhu, B. Mohanty, and H. Xie, "Numerical investigation of blasting-induced crack initiation and propagation in rocks," *Int. J. Rock Mech. Mining Sci.*, vol. 44, no. 3, pp. 412–424, Apr. 2007, doi: 10.1016/j.ijrmms.2006.09.002.

[24] A. Rouabhi, M. Tijani, P. Moser, and D. Goetz, "Continuum modelling of dynamic behaviour and fragmentation of quasi-brittle materials: Application to rock fragmentation by blasting," *Int. J. Numer. Anal. Methods Geomech.*, vol. 29, no. 7, pp. 729–749, Jun. 2005, doi: 10.1002/nag.436.

[25] G. W. Ma and X. M. An, "Numerical simulation of blasting-induced rock fractures," *Int. J. Rock Mech. Mining Sci.*, vol. 45, no. 6, pp. 966–975, Sep. 2008, doi: 10.1016/j.ijrmms.2007.12.002.

[26] A. Karrech, C. Schrank, R. Freij-Ayoub, and K. Regenauer-Lieb, "A multi-scaling approach to predict hydraulic damage of poromaterials," *Int. J. Mech. Sci.*, vol. 78, pp. 1–7, Jan. 2014.

[27] X. Dong, A. Karrech, H. Basarir, M. Elchalakani, and A. Seibi, "Energy dissipation and storage in underground mining operations," *Rock Mech. Rock Eng.*, vol. 52, no. 1, pp. 229–245, 2018.

[28] Z. Aliabadian, G.-F. Zhao, and A. R. Russell, "Crack development in transversely isotropic sandstone discs subjected to Brazilian tests observed using digital image correlation," *Int. J. Rock Mech. Mining Sci.*, vol. 119, pp. 211–221, Jul. 2019, doi: 10.1016/j.ijrmms.2019.04.004.

[29] X. HZ, Z. QB, B. CH, B. Pan, and J. Zhao, "High-speed photography and digital optical measurement techniques for Geomaterials: Fundamentals and applications," *Rock Mech. Rock Eng.*, vol. 50, pp. 1611–1659, Feb. 2017, doi: 10.1007/s00603-016-1164-0.
[30] X.-P. Zhou, Y.-T. Wang, J.-Z. Zhang, and F.-N. Liu, "Fracturing behavior study of three-flawed specimens by uniaxial compression and 3D digital image correlation: Sensitivity to brittleness," *Rock Mech. Rock Eng.*, vol. 52, no. 3, pp. 691–718, Mar. 2019, doi: 10.1007/s00603-018-1600-4.
[31] Q. Zhu, D. Li, Z. Han, X. Li, and Z. Zhou, "Mechanical properties and fracture evolution of sandstone specimens containing different inclusions under uniaxial compression," *Int. J. Rock Mech. Mining Sci.*, vol. 115, pp. 33–47, Mar. 2019, doi: 10.1016/j.ijrmms.2019.01.010.
[32] D. Li, F. Gao, Z. Han, and Q. Zhu, "Experimental evaluation on rock failure mechanism with combined flaws in a connected geometry under coupled static-dynamic loads," *Soil Dyn. Earthq. Eng.*, vol. 132, May 2020, Art. no. 106088, doi: 10.1016/j.soildyn.2020.106088.
[33] M. Tao, X. Li, and C. Wu, "3D numerical model for dynamic loading-induced multiple fracture zones around underground cavity faces," *Comput. Geotechnics*, vol. 54, pp. 33–45, Oct. 2013.
[34] Z. Zhu, C. Wang, J. Kang, Y. Li, and M. Wang, "Study on the mechanism of zonal disintegration around an excavation," *Int. J. Rock Mech. Mining Sci.*, vol. 67, pp. 88–95, Apr. 2014, doi: 10.1016/j.ijrmms.2013.12.017.
[35] T. J. Holmquist and G. R. Johnson, "A computational constitutive model for glass subjected to large strains, high strain rates and high pressures," *J. Appl. Mech.*, vol. 78, no. 5, Sep. 2011, doi: 10.1115/1.4004326.
[36] M. M. D. Banadaki, "Stress-wave induced fracture in rock due to explosive action," *Lille Médical J La Fac Médecine Pharm Luniversité Lille.*, vol. 24, no. 4, pp. 283–286, 2011.
[37] Y. B. Xiong, Y. L. Hu, J. Xu, and J. J. Chen, "Determining failure surface parameters of the Johnson-Holmquist concrete constitutive model," *Binggong Xuebao/Acta Armamentarii*, vol. 31, no. 6, pp. 746–750, 2010.

CHENGLONG HE was born in Taiyuan, Shanxi, China. He received the Ph.D. degree from the State Key Laboratory of Explosion Science and Technology, Beijing Institute of Technology, Beijing, China, in 2018. He is a member of the International Society of Rock Mechanics and Rock Engineering (ISRM). His main research interests include the dynamic response of rock material under impact loading or blasting. He received the Science and Technology Progress Award from the China Society of Engineering Blasting in 2015. He presented as Oral Presentation during the 14th International Congress on Rock Mechanics and Rock Engineering, held in Foz do Iguassu, Brazil, in September 2019.

JINMING GAO was born in Dezhou, Shandong, China. He received the master's degree from the State Key Laboratory of Explosion Science and Technology, Beijing Institute of Technology, Beijing, China, in 2018. His research interests include the stress wave propagation and the material dynamic response by SHPB compression experiment.

DAYONG CHEN was born in Minquan, Henan, China. He received the Ph.D. degree from the State Key Laboratory of Explosion Science and Technology, Beijing Institute of Technology, Beijing, China, in 2012. His research interests include the green mining related research work, especially in blasting, rock control, dynamic disaster, and other aspects of more exploration.

JIANGUANG XIAO was born in Zhumadian, Henan, China. He received the master's degree from the State Key Laboratory of Explosion Science and Technology, Beijing Institute of Technology, Beijing, China, in 2016. His research interest includes failure and ejection behaviour of concrete materials under internal blast loading.